Journal of Biomechanics xxx (2018) xxx–xxx

Contents lists available at ScienceDirect

Journal of Biomechanics

journal homepage: www.elsevier.com/locate/jbiomech
www.JBiomech.com

Analysis of surface-to-surface distance mapping during three-dimensional motion at the ankle and subtalar joints

Sorin Siegler [a,*], Tobias Konow [a,b], Claudio Belvedere [c], Andrea Ensini [c], Rewati Kulkarni [a], Alberto Leardini [c]

[a] Department of Mechanical Engineering and Mechanics, Drexel University, Philadelphia, PA, USA
[b] Institute of Biomechanics, Hamburg University of Technology, Hamburg, Germany
[c] Movement Analysis Laboratory, Istituto Ortopedico Rizzoli, Bologna, Italy

ARTICLE INFO

Article history:
Accepted 30 May 2018
Available online xxxx

Keywords:
Ankle joint
Subtalar joint
Surface-to-surface distance mapping
Three-dimensional kinematics

ABSTRACT

Joint surface interaction and ligament constraints determine the kinematic characteristics of the ankle and subtalar joints. Joint surface interaction is characterized by joint contact mechanics and by relative joint surface position potentially characterized by distance mapping. While ankle contact mechanics was investigated, limited information is available on joint distance mapping and its changes during motion. The purpose of this study was to use image-based distance mapping to quantify this interaction at the ankle and subtalar joints during tri-planar rotations of the ankle complex. Five cadaveric legs were scanned using Computed Tomography and the images were processed to produce 3D bone models of the tibia, fibula, talus and calcaneus. Each leg was tested on a special linkage through which the ankle complex was loaded in dorsiflexion/plantarflexion, inversion/eversion, and internal/external rotation and the resulting bone movements were recorded. Fiduciary bone markers data and 3D bone models were combined to generate color-coded distance maps for the ankle and subtalar joints. The results were processed focusing on the changes in surface-to-surface distance maps between the extremes of the range of motion and neutral. The results provided detailed insight into the three-dimensional highly coupled nature of these joints showing significant and unique changes in distance mapping from neutral to extremes of the range of motion. The non-invasive nature of the image-based distance mapping technique could result, after proper modifications, in an effective diagnostic and clinical evaluation technique for application such as ligament injuries and quantifying the effect of arthrodesis or total ankle replacement surgery.

1. Introduction

The complex kinematics and stiffness characteristics of the ankle and subtalar joints are the result of surface-to-surface interaction between the articulating joint surfaces (Stormont et al., 1985, Tochigi et al., 2006) and the restraining action of the surrounding ligaments (Siegler et al., 1988, Leardini et al., 1999a, 1999b). Motivated by the need to establish reliable diagnostic techniques for ankle ligament injuries several investigators studied the stabilizing role of the surrounding ligaments primarily in vitro using ligament sectioning techniques (Lapointe et al., 1997, Ringleb et al., 2005). However, data on the surface-to-surface interaction at the ankle and subtalar joints are limited and incomplete. This, despite the fact that such data are essential for a variety of clinical applications such as optimizing arthrodesis and the design and evaluation of artificial articulations for effective total ankle replacements required for treatment of severe ankle osteoarthritis (Giannini et al. 2000, Espinosa and Klammer, 2010).

The surface-to-surface interaction at a joint can be divided into two major inter-related components. One component is the contact locations and surface pressure distribution between the articulating surfaces. These properties were studied in the past for the ankle joint using pressure sensitive Fuji film (Kimizuka et al., 1980, Calhoun et al., 1994) recording peak pressure distribution and areas of contact across the joint surfaces in different joint positions. The second component is the spatial relationship between the articular surfaces during joint motion (Corazza et al., 2005). This property may be characterized through distance maps that describe the dis-

* Corresponding author at: Department of mechanical Engineering and Mechanics, Drexel University, 32nd and Chestnut Streets, Philadelphia, PA 19104, USA.
E-mail address: ssiegler@coe.drexel.edu (S. Siegler).

https://doi.org/10.1016/j.jbiomech.2018.05.026
0021-9290/

tribution of distances between the articulating surfaces at each joint position. Corazza et al. (2005) investigated this property of surface-to-surface interaction at the ankle joint for dorsiflexion/-plantarflexion motion in vitro. This was done by directly digitizing a small number of points on each articulating surface and following the changes in distance between corresponding points during motion. This study provided an incomplete description of surface-to-surface characteristics since it was limited to a small number of points on the articulating surface, was limited to dorsiflexion/-plantarflexion only and did not include the subtalar joint.

The goal of this study was to characterize the surface-to-surface interaction at the ankle and subtalar joints, using an image-based distance mapping approach, at neutral and at extreme positions in its reachable three-dimensional space of the ankle complex. It expands on the studies described earlier by using a large number of points on the articulating surfaces as obtained from 3D models of the bones produced from high-resolution CT scans. It also includes the subtalar joint for which such data is presently unavailable, and it explores the surface-to-surface interaction for the full three-dimensional functional range of motion of the ankle complex.

2. Materials and methods

2.1. Specimen preparation

The study was conducted on five fresh cadaver legs, free from anatomical defects, disarticulated at the knee, obtained from five subjects (3 males, 2 females) with an average age of 53.6 years. Following thawing and inspection by an orthopedic surgeon to ensure lack of pathologies, three fiduciary holes (2 mm diameter and approximately 5 mm deep) were drilled into each bone: the tibia, talus, and calcaneus. Polymeric plugs (2mm diameter and 5 mm long) were press fitted into each fiduciary hole such that one end of the plug was flush with the surface of the bone for easy identification and marking. The leg was then scanned through a Computed Tomography system (Brilliance CT 16-slice system by Philips Healthcare) with an in-plane resolution of 0.15 mm by 0.15 mm and an inter-slice distance of 0.4 mm.

2.2. Testing procedure

Each specimen was mounted and aligned into a six-degrees-of-freedom linkage (Fig. 1), the Ankle Flexibility Tester - AFT. During the initial alignment procedure, the foot was compressed manually by a force of approximately 5 N against the footplate of the AFT to insure good conformity between the plantar aspect of the foot and the footplate. The device, described in early publications (Ringleb et al., 2005, Siegler et al., 2005, Belvedere et al., 2017), enabled application and measurement of torques across the ankle complex. The continuous torques were applied, measured, and recorded through a torque applicator with a torque sensor mounted on it shaft (Fig. 1). The motion produced at the ankle and subtalar joint in response to these torques was recorded using an optoelectronic stereo-photogrammetric motion acquisition system (Stryker Knee Navigation System, Stryker®, Kalamazoo, MI-USA). For this purpose, four bone trackers, each containing five LED position markers were used. Each tracker could record the six-degrees-of-freedom motion of the corresponding bone, considered rigid, with a positional accuracy of 0.2 mm and a rotational accuracy of 0.5 degrees (Sparmann et al., 2003, Belvedere et al., 2014). Each of three trackers were fixed in convenient accessible locations on the bones, one to the tibia, one to the talus, and one to the calcaneus (Fig. 1). The three trackers recorded the motion of these bones as torques were applied manually through the AFT to produce movements in dorsiflexion/plantarflexion, inversion/eversion, and internal/external rotation. Torque and kinematic data were synchronized and collected on a computer at a rate of 20 samples per second.

In the first test, motion was produced over the entire range of motion of the ankle complex in flexion/extension by manually loading the ankle complex through the AFT with a torque in the sagittal plane, without the use of the torque sensor. No torque sensor was used due to the large flexibility of the joint complex in this rotational direction. In the subsequent tests, motion was produced at the ankle complex by manually applying torques through the instrumented torque sensor (Fig. 1) about the inversion/eversion and internal/external rotation axes of the AFT (Siegler et al., 1996). These torques were applied starting from three different

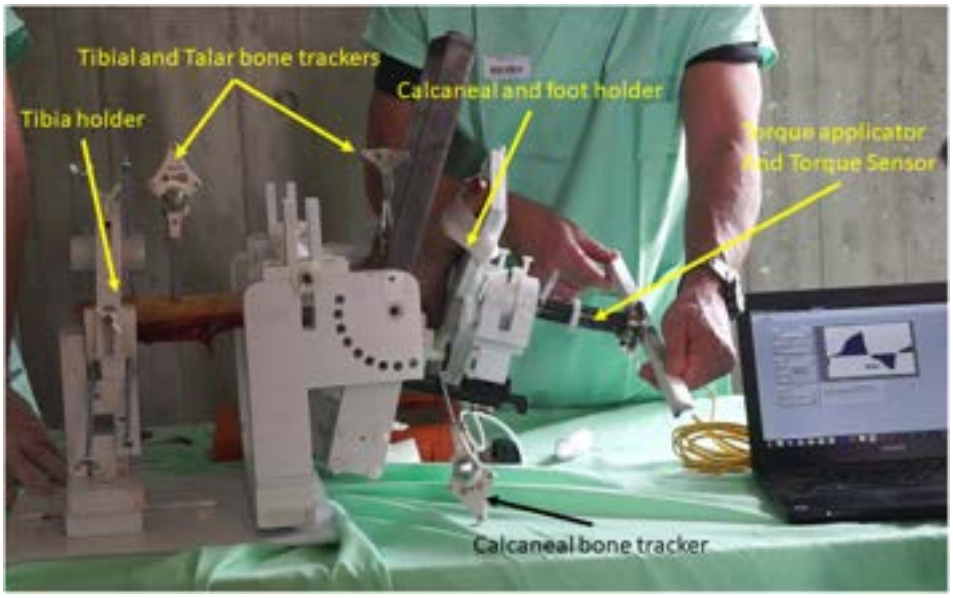

Fig. 1. Experimental setup showing testing of one specimen. The specimen is aligned and fixed in the AFT through the tibial holder and the foot plate. Loading was applied manually and recorded through a torque sensor. Motion of the tibia, talus and calcaneus was recorded through the optoelectronic bone trackers (Stryker Knee Navigation System, Stryker®, Kalamazoo, MI-USA).

Please cite this article in press as: Siegler, S., et al. Analysis of surface-to-surface distance mapping during three-dimensional motion at the ankle and subtalar joints. J. Biomech. (2018), https://doi.org/10.1016/j.jbiomech.2018.05.026

joint positions within the flexion arc, i.e. the neutral (Neutral), the maximum dorsiflexion (MaxDorsi), and maximum plantarflexion (MaxPlantar). At least four loading-unloading cycles, reaching peak torques of 3.4 N m in all directions, were applied in each test at a slow rate of approximately five cycles per minute. This value of maximum torque ensured reaching the end of the range of motion with no damage to the specimen and ensured minimal cycle-to-cycle variations.

Experimental testing of each specimen was concluded by a "calibration" procedure in which the fourth tracker was used as a spatial landmark digitizer to record the position of the center of the fiduciary holes on the surface of the bones relative to the corresponding tracker reference frame. These data were used to register the bone models obtained from the CT scans to the position of the bones during their motion under the applied torques. Also, the location of anatomical landmarks relative to the bone tracker's reference frame were identified using the digitizer in order to establish reference frames to describe the motion at the ankle, subtalar, and ankle complex (Cappozzo et al., 1995).

Validity and accuracy of the distance map algorithm were tested by CT scanning two polymeric cylindrical phantoms positioned relative to each other in two different known configurations and obtaining the surface-to-surface distance for a large number of surface points through the present distance-mapping technique. These distances were compared to theoretical distance values to obtain error distribution. Full description is provided in the Supplemental Materials.

2.3. Data processing and statistical analysis

Images were imported into an image processing software (Analyze Direct™, Overland Park, KS-USA) to produce 3D models of the articulating bones and of the fiduciary holes, after proper segmentation, 3D filtering and rendering. The 3D bone surface renderings were smoothed with a spatial filter (GEOMAGIC CONTROL™, Morrisville, NC-USA) to remove minor irregularities. A 2-millimeter diameter cylinder was then optimally fitted to each fiduciary hole. The intersection of the long axis of each fiduciary cylinder and the surface of the bone was marked as a fiduciary point, resulting in three fiduciary points on the surface of each bone (Fig. 2).

The relative position between the bones at each time increment was obtained by registering the position data of the fiduciary points obtained from the 3D data rendering from the CT images with the position data of the fiduciary points from the bone tracker. Once the relative bone position was established through, a distance-mapping algorithm (GEOMAGIC CONTROL™, Morrisville, NC-USA) was used to compute and visualize the distances between the articulating surfaces at the ankle and the subtalar joint for each time increment. Surface-to-surface distance was defined and calculated as the shortest distance from each point on one surface to the opposite. Using the kinematic data, the neutral and the extreme positions in each direction for each cyclic loading were identified and the distance maps in these positions were used in the subsequent analysis. For the ankle joint, the distance maps were obtained separately for the articulations between the talar dome and the tibial plafond, and between the medial and lateral sides of the talus and the corresponding malleoli. The distance results were displayed as color-coded maps on the surface of each articulating bone (Fig. 3). Each color depicts a different surface-to-surface distance range. Twenty-three colors were used to describe the distance map in the overall range of −1 mm to +4 mm (Fig. 3). The negative numbers represent surface penetration, a physical impossibility, but possible in the distance maps due to system errors.

The surfaces of the ankle and subtalar joints were subdivided into sub-regions to quantify the effect of motion on surface-to-surface distance maps and to allow statistical inter-specimen analysis. It was essential to ensure that the division of the articular surfaces into sub-regions was consistent both across change in position (neutral to extremes) and across specimens. Therefore, the division of the articular surfaces into sub-regions was performed as follows.

Guided by anatomical atlas (Kelikian, 2011) and by previous observations from cadaver ankle dissection, the boundaries of the superior, medial and lateral articular surfaces of the talus, for the ankle joint, and of the superior articular surfaces of the calcaneus, for the subtalar joint, were identified and marked on each of the 3D bone models. This resulted in three distinct regions for the talus including the talar dome, for the articulation with the tibial plafond, the medial side region where it articulates with the interior of the tibial medial malleolus, and the lateral side region where it articulates with the fibular lateral malleolus (Fig. 4). Two distinct articular regions were identified for the subtalar joint on the superior side

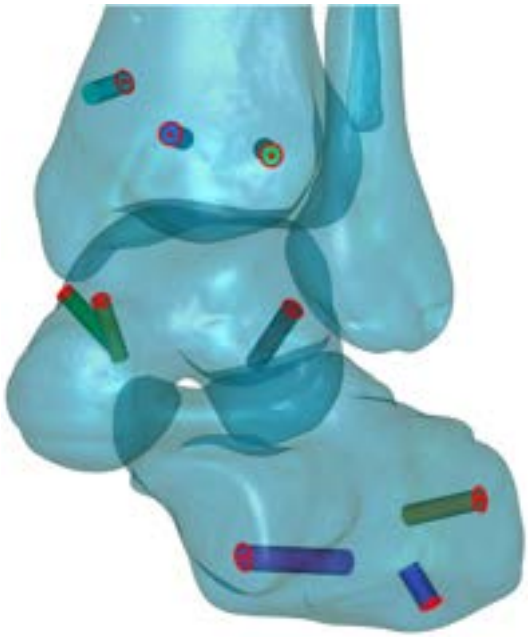

Fig. 2. View of the 3D renderings of the bones including the fiduciary holes represented as cylinders. The fiduciary points used in the analysis were the center of circles obtained as the intersection of the long axis of the cylinder and the surface of the bone.

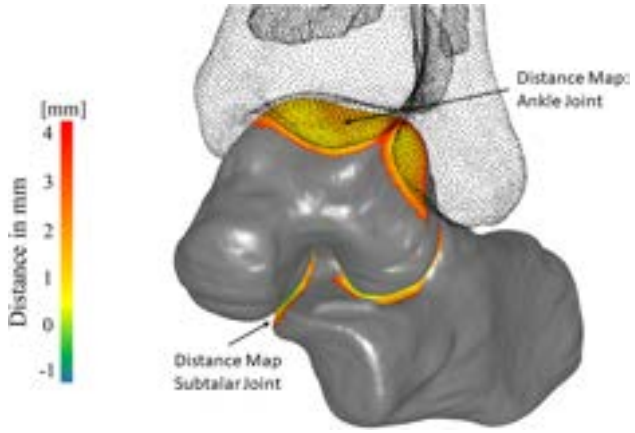

Fig. 3. Image of the 3D renderings of the bones showing the color-coded distance maps on the surface of the talus for the ankle joint and on the surface of the calcaneus for the subtalar joint. Distances are shown in millimeters.

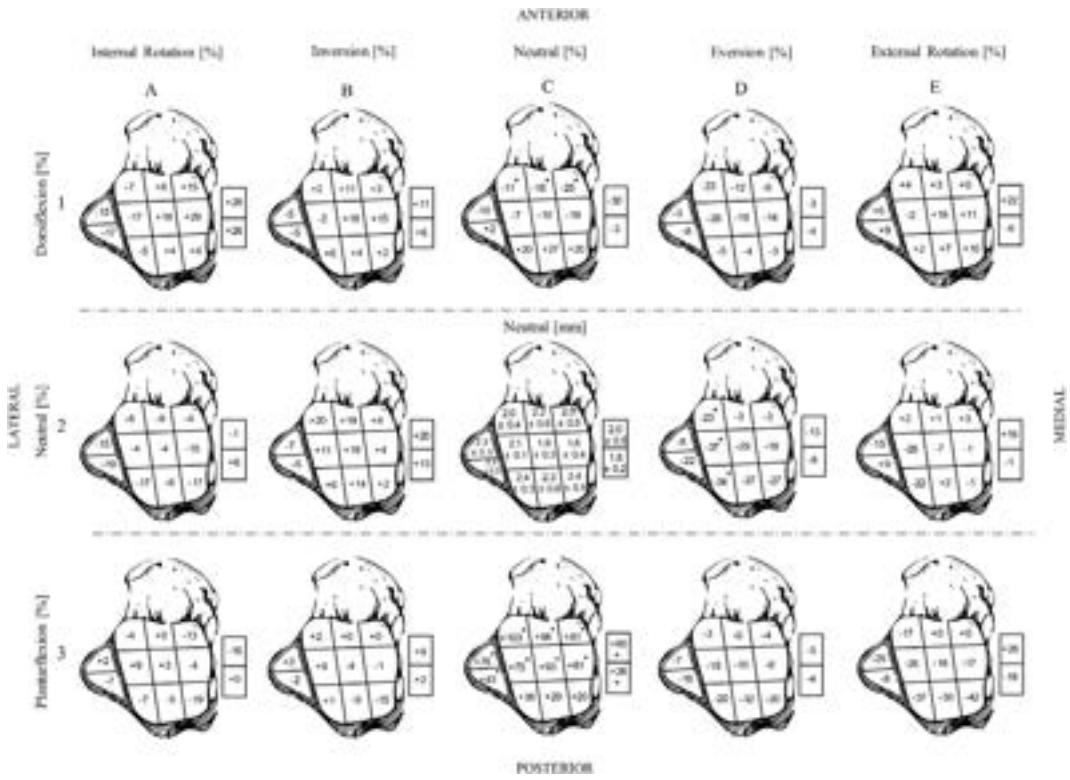

Fig. 4. Transverse superior views of the talus with the articulating surfaces divided into nine sub-regions on the talar dome and two each on the medial and lateral side surfaces of the talus where it articulates with the inside surfaces of the malleoli. The average distances and associated standard deviations are indicated in millimeters for each sub-region for the neutral position in cell C2 marked "Neutral [mm]". The changes, in percentage, from neutral to the extreme positions of dorsiflexion or plantarflexion are indicated in cells C1 and C3. The change, in percentage, from neutral to inversion or eversion are shown in Cells B2 and D2 and to internal rotation or external rotation in cell A2 and E2. The changes, in percentage, in these directions, starting from dorsiflexion or plantarflexion are shown in the corresponding cells of row 1 and row 3. (*) indicates statistical significance in a sub-region ($p < 0.05$) compared to the starting position in the same sub-region.

of the calcaneus. A posterior articular surface and an anterior articular surface on the sustentaculum tali (Fig. 5). Once these regions were identified and their boundaries marked, the bone models were converted into point clouds and all the surface points within the previously marked boundaries were marked so that their location could be identified in any position. For each of the five articular regions, a least square error algorithm was used to fit a plane through all the marked point within the region. After this plane was created each marked point on the articular surface was projected onto the optimally fitted plane. This produced a consistent and motion invariant two-dimensional projection of the articular surfaces so that every marked point an articular surface had a fixed unique position on the best-fitted plane that was invariant under change in position of the joint. Using this technique, the distance maps from the sub-regions could be compared for different joint positions and across specimens. Each of the five articular surfaces were divided into a small number of sub regions of equal areas in order to allow statistical comparison between specimens and to identify, on a statistical basis, the difference between different joint positions. The talar dome was divided into nine sub-regions, the medial and lateral sides of the talus were divided into two sub-regions each (Fig. 4), the posterior articular surface of the calcaneus was divided into six sub-regions and the sustentaculum tali was divided into two sub-regions (Fig. 5). For each sub-region, the mean surface-to-surface distance for all points within the sub-region, and associated standard deviation, were computed.

Using the average surface-to-surface distances from the sub-regions, the cycle-to-cycle repeatability in the distance maps was examined for three different joint positions, neutral, maximum dorsiflexion, and maximum plantarflexion. From these, the average and standard deviation for the cycle-to-cycle variability and the maximum cycle-to-cycle errors were computed. To compare the effect of motion from neutral to the extremes of range of motion across the five specimens, a repeated-measure, one-way analysis of variance (ANOVA) was employed with the significant probability level set at $p < 0.05$. When significant differences were detected, a Bonferroni post hoc test was used to identify the groups that were statistically different from each other (these are marked in Fig. 4 and Fig. 5 with a * - symbol).

3. Results

The validation test performed on the two cylindrical phantoms (see Supplemental Materials) produced for the two tested configurations average errors of 0.538 mm and 0.197 mm, and a maximum overall error of 0.654 mm. The cycle-to-cycle intra-specimen variability in the distance maps as calculated from the sub-region divisions for the ankle joint for the three representative positions of neutral, maximum dorsiflexion and maximum plantarflexion averaged 0.07 mm with a standard deviation of 0.065 mm and a maximum error of 0.2 mm.

The average distances, for each sub-region, averaged over all specimens, and the associated standard deviations, are indicated in millimeters for the neutral position in cell C2 marked "Neutral [mm]" in Figs. 4 and 5. The changes, in percentage, from a starting position of either neutral, dorsiflexion or plantarflexion to extreme positions of inversion/eversion or internal or external rotations are indicated in the rest of the cells in Figs. 4 and 5.

All five specimens produced consistently similar distance maps variations from neutral to the different extreme positions.

Please cite this article in press as: Siegler, S., et al. Analysis of surface-to-surface distance mapping during three-dimensional motion at the ankle and subtalar joints. J. Biomech. (2018), https://doi.org/10.1016/j.jbiomech.2018.05.026

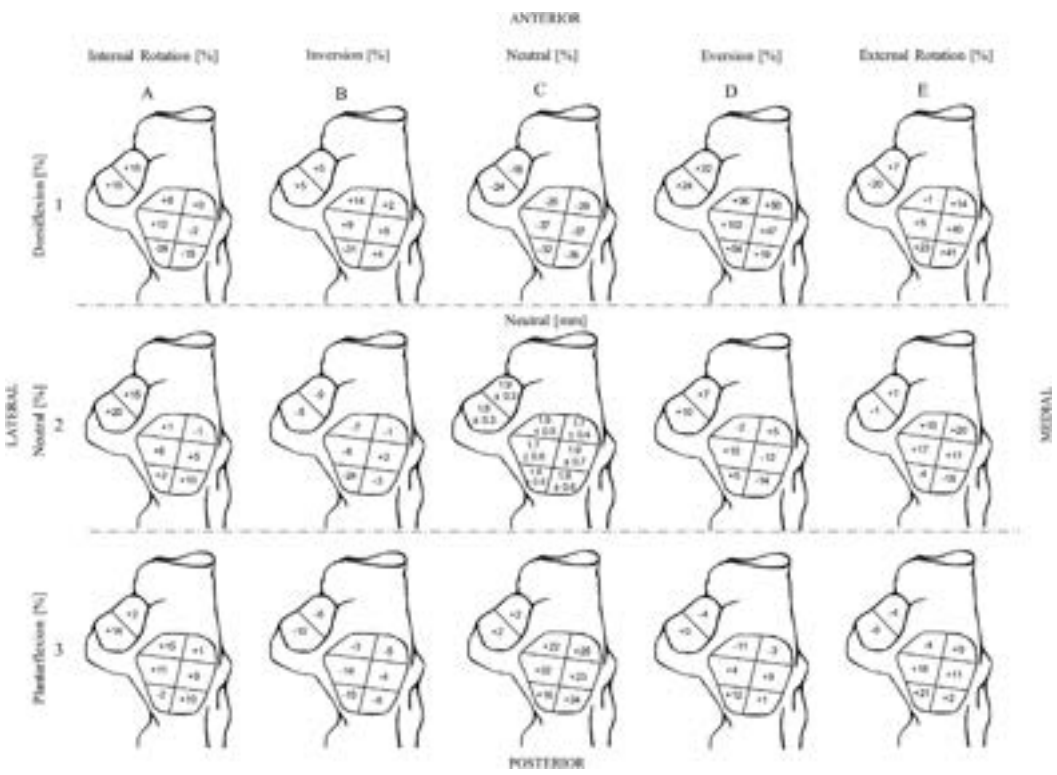

Fig. 5. Transverse superior views of the calcaneus with the articulating surfaces divided into six sub-regions for the posterior articulating surface of the subtalar joint and two sub-regions on the surface of the sustentaculum tali. The average distances and associated standard deviations are indicated in millimeters for each sub-region for the neutral position in cell C2 marked "Neutral [mm]". The changes, in percentage, from neutral to the extreme positions of dorsiflexion or plantarflexion are indicated in cells C1 and C3. The change, in percentage, from neutral to inversion or eversion are shown in Cells B2 and D2 and to internal rotation or external rotation in cell A2 and E2. The changes, in percentage, in these directions, starting from dorsiflexion or plantarflexion, are shown in the corresponding cells of row 1 and row 3. (*) indicates statistical significance in a sub-region ($p < 0.05$) compared to the starting position in the same sub-region.

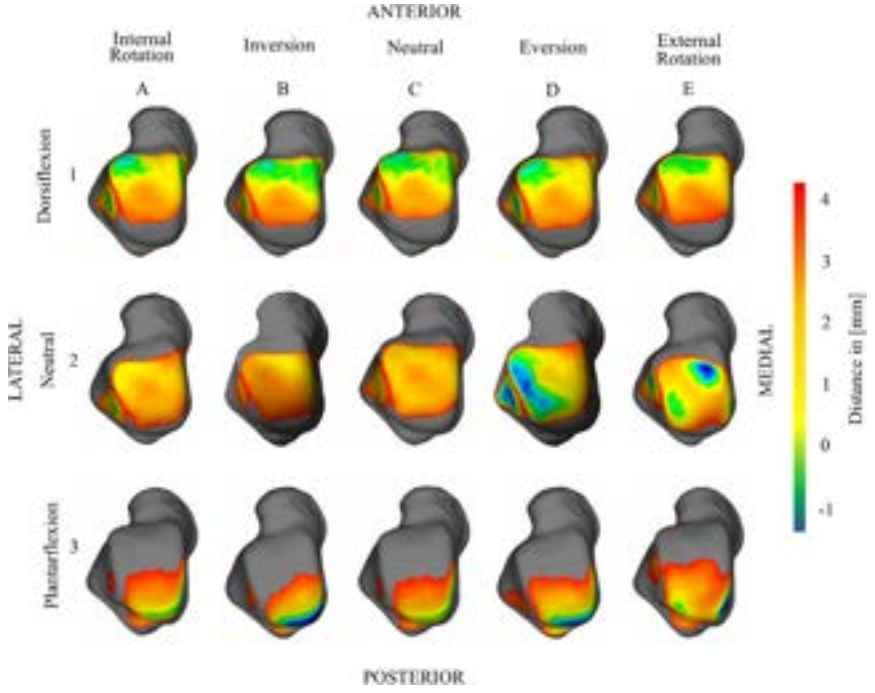

Fig. 6. Transverse superior views of the talus for one specimen showing the color-coded distance maps at the ankle joint. Rows are marked by numbers (1, 2, 3) and columns by letters (A, B, C, D, E) and each cell corresponds to a different joint position. For example, cell C2 corresponds to neutral, element C3 corresponds to plantarflexion, and cell B1 corresponds to inversion starting from dorsiflexion.

Please cite this article in press as: Siegler, S., et al. Analysis of surface-to-surface distance mapping during three-dimensional motion at the ankle and subtalar joints. J. Biomech. (2018), https://doi.org/10.1016/j.jbiomech.2018.05.026

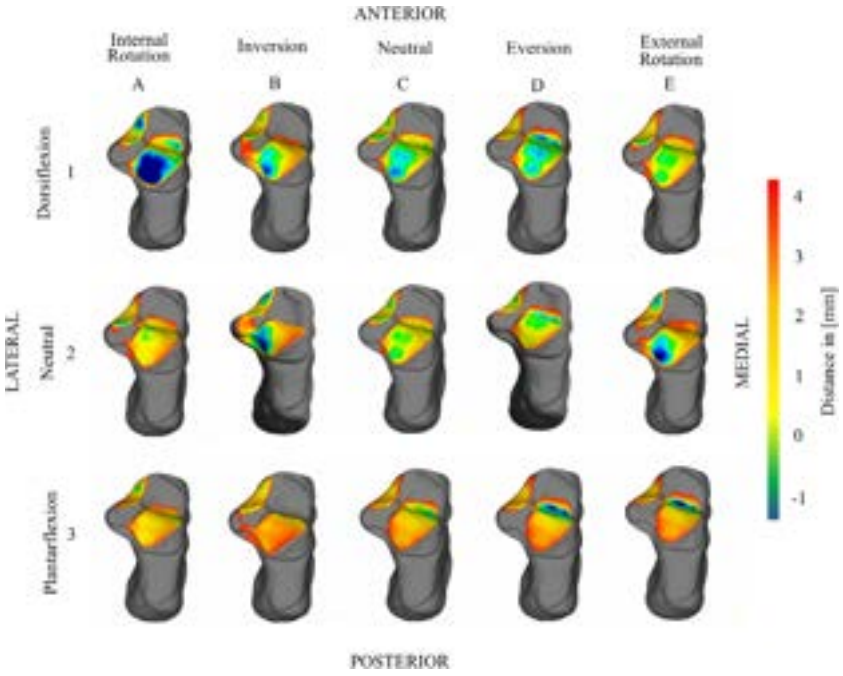

Fig. 7. Transverse superior views of the calcaneus for one specimen showing the color-coded distance maps at the subtalar joint. Rows are marked by numbers (1, 2, 3) and columns by letters (A, B, C, D, E) and each cell corresponds to a different joint position. For example, cell C2 corresponds to neutral, element C3 corresponds to plantarflexion, and cell B1 corresponds to inversion starting from dorsiflexion.

Therefore, the full distance map results obtained from one specimen (Figs. 6 and 7) and the relative bone positions in neutral and extreme positions (Fig. 8) are typical and representative of all specimens and show similar variations to those obtained based on inter-specimen averaging in the sub-regions.

In neutral, no statistically significant differences were found between the various sub-regions for either the ankle joint or for the subtalar joint (cell C2 in Figs. 4 and 5) indicating high level of congruity between all the articulating joint surfaces in this position.

Statistically significant differences in the distance maps were observed between neutral and the extreme positions of maximum dorsiflexion (C1 to C2 in Fig. 4) and maximum plantarflexion (C3 to C2 in Fig. 4). Specifically, in dorsiflexion the three anterior sub-regions of the talar dome were significantly closer to the tibial plafond than in neutral while in plantarflexion the anterior and central sub-regions of the talar dome as well as all sub-regions at the articulations with the medial and lateral malleoli were significantly further away from the tibial plafond than in neutral. This was also observed qualitatively in Fig. 6 (compare cells C1 to C2 and C3 to C2) and Fig. 8. No statistical significant differences were observed between dorsiflexion and neutral or plantarflexion and neutral at the subtalar joint (Fig. 5). In eversion, statistically significant differences and qualitative differences (D2 to C2 in Fig. 4) were observed at the ankle joint between eversion and neutral in the three lateral sub-regions of the talar dome. No statistical significant differences occurred between inversion or eversion and neutral at the subtalar joint or between inversion and neutral at the ankle joint. In internal rotation and external rotation no significant changes in the distance maps compared to neutral were observed either at the ankle or at the subtalar joints. When the ankle complex was in dorsiflexion or plantarflexion, surface-to-surface distance changes between inversion, eversion, internal rotation and external rotation, compared to the starting dorsiflexed or plantarflexed position were statistically insignificant.

4. Discussion

Highly repeatable cycle-to-cycle distance maps were produced at the ankle and subtalar joint providing further indication of the reliability of the distance mapping technique.

As the ankle changes position from neutral to dorsiflexion, the anterior parts of the talar dome approach the tibial plafond and those regions, including the central regions of the talar dome, move away from the tibial plafond in plantarflexion. This finding supports the conclusion of previous studies (Chen et al., 1988, Lundberg et al. 1989, Calhoun et al., 1994, Leardini et al., 1999a, 1999b; Corazza et al., 2005, Kelikian, 2011) that the ankle does not have a fixed axis of rotation, in which case the articular surfaces would have maintained full congruity, but rather acts as a sliding and rolling joint with the contact regions moving from posterior to anterior locations as the ankle complex moves from plantarflexion to dorsiflexion. In addition, the significant separation, compared to neutral, between the sides of the talus and the interior of the medial and lateral malleoli is consistent with the wedge shaped talus having its anterior part wider than the posterior part (Kelikian, 2011). This interaction between the wedge-shaped talus and the lateral and medial malleoli has been described qualitatively in earlier publications but has not been directly demonstrated and quantified before.

The results indicate that as the ankle changes position from neutral to eversion, the lateral parts of the articular surface on the talar dome approach the tibial plafond. These findings are in agreement with Calhoun et al. (Calhoun et al., 1994) in their pressure distribution studies using Fuji film technology.

This study had several limitations. The number of specimens was small and therefore generalization of the results must be done with caution, particularly due to the previously observed and documented large inter-specimen variations. Additionally, the use of CT images produced distance maps between the subchondral bones and not between the articulating joint cartilage surfaces.

Please cite this article in press as: Siegler, S., et al. Analysis of surface-to-surface distance mapping during three-dimensional motion at the ankle and subtalar joints. J. Biomech. (2018), https://doi.org/10.1016/j.jbiomech.2018.05.026

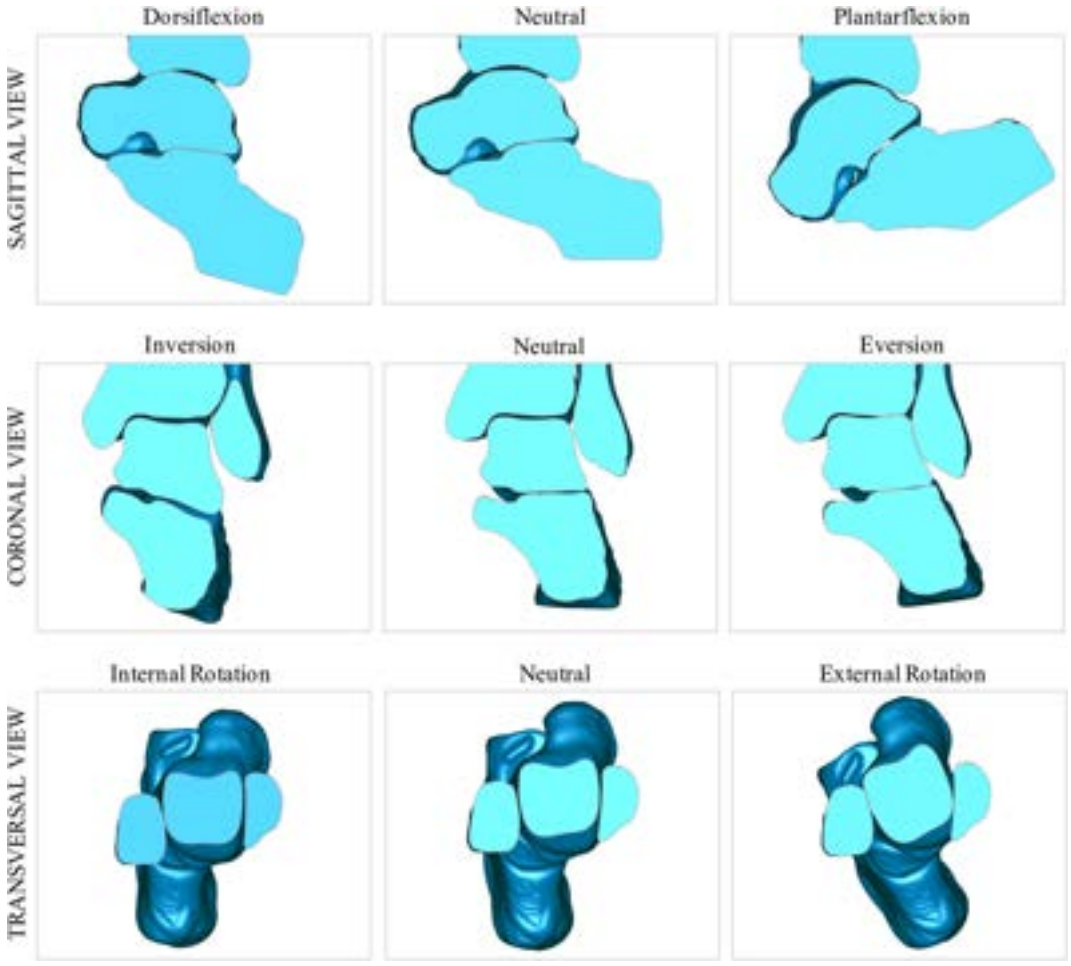

Fig. 8. Sagittal, coronal and transverse sections through the ankle complex showing the relative position between the bones at the ankle and subtalar joint in neutral and at the extremes position of the ankle complex of dorsiflexion, plantarflexion, inversion, eversion, internal rotation, and external rotation.

Also, as indicated earlier, the distance map algorithm may produce negative numbers represent surface penetration, a physical impossibility. However, penetration regions in the distance maps may occur at and near contact locations where the combined thickness of the articular cartilage is smaller than the error in the distance maps. The estimated distance map error includes voxel resolution in the CT images of the order of 0.45 mm and the positional error from the surgical navigation system of 0.2 mm resulting in a potential error in the distance map of the order of 0.65 mm on each surface for a potential maximum error in distance at a specific location of 1.3 mm. Articular cartilage at the ankle was reported to vary from as low as 0.5 mm to as high as 1.8 mm (Sugimoto et al., 2005, Millington et al., 2007a, 2007b) resulting in potential combined thickness at contact locations below the distance maps error and indicate in the distance maps as penetration. These limitations were partially addressed by the use of repeated measure experimental design and statistical analysis since the primary focus of the study was on the changes in surface-to-surface distance maps that occur between neutral and the extreme ankle complex positions and not on the absolute values of these distances in millimeters. Another limitation was the high dose of radiation required to achieve the present high scan resolution. While this was not a problem in the present study performed on cadavers, it may represent a challenge when adopting this technique to in-vivo measures, in standard clinical settings. However, for such conditions, high resolution MRI or cone beam CT, which implies only a fraction of radiation dose of conventional CT, could be used. Finally, the validation of the present distance mapping technique was performed under idealized conditions (cylinders in air). Future studies may require expanding this validation process by using phantoms of more realistic anatomical structures.

It should be emphasized that this study characterized the changes in joint surface interaction between neutral and the extremes of the range of motion and not during simulated functional activities such as walking. Therefore, while a small axial load was maintained during the experiments, the axial loads and the joint kinematics typical of functional activities were not reproduced. Therefore, the present study provides only distance maps for the ankle under conditions where the effect of compressive loads, such as result during weight bearing activities, is not included. These results provide the necessary base-line data for future studies where the effect of axial loading, representing weight bearing conditions, are investigated.

The present study provides, for the first time, a detailed insight into the interaction of the articulating surfaces in healthy ankle and subtalar joints at neutral and at extreme joint positions. This limited normal baseline, which will be expanded in the future, may be used to evaluate various ankle pathologies and treatment techniques by assessing their ability to restore normal surface-to-surface interaction at these joints. In addition, the technique may be modified and adopted for in vivo applications as an image-based diagnostic and post-treatment evaluation procedure. This could be achieved by scanning the ankle in specific stressed positions such as under axial load using weight-bearing CT.

Please cite this article in press as: Siegler, S., et al. Analysis of surface-to-surface distance mapping during three-dimensional motion at the ankle and subtalar joints. J. Biomech. (2018), https://doi.org/10.1016/j.jbiomech.2018.05.026

Acknowledgment

This study was support by a grant from the Coulter-Drexel Translational Research Partnership.

Conflict of interest

None.

Appendix A. Supplementary material

Supplementary data associated with this article can be found, in the online version, at https://doi.org/10.1016/j.jbiomech.2018.05.026.

References

Belvedere, C., Ensini, A., Leardini, A., Dedda, V., Feliciangeli, A., Cenni, F., Timoncini, A., Barbadoro, P., Giannini, S., 2014. Tibio-femoral and patello-femoral joint kinematics during navigated total knee arthroplasty with patellar resurfacing. Knee Surg. Sports Traumatol. Arthrosc. 22 (8), 1719–1727.

Belvedere, C., Siegler, S., Ensini, A., Toy, J., Caravaggi, P., Namani, R., Giannini, G., Durante, S., Leardini, A., 2017. Experimental evaluation of a new morphological approximation of the articular surfaces of the ankle joint. J. Biomech. 53, 97–104.

Calhoun, J.H., Li, F., Ledbetter, B.R., Viegas, S.F., 1994. A comprehensive study of pressure distribution in the ankle joint with inversion and eversion. Foot. Ankle Int. 15 (3), 125–133.

Cappozzo, A., Catani, F., Croce, U.D., Leardini, A., 1995. Position and orientation in space of bones during movement: anatomical frame definition and determination. Clin. Biomech. (Bristol., Avon.) 10 (4), 171–178.

Chen, J., Siegler, S., Schneck, C.D., 1988. The three-dimensional kinematics and flexibility characteristics of the human ankle and subtalar joint–Part II: Flexibility characteristics. J. Biomech. Eng. 110 (4), 374–385.

Corazza, F., Stagni, R., Castelli, V.P., Leardini, A., 2005. Articular contact at the tibiotalar joint in passive flexion. J. Biomech. 38 (6), 1205–1212.

Espinosa, N., Klammer, G., 2010. Treatment of ankle osteoarthritis: arthrodesis versus total ankle replacement. Eur. J. Trauma Emerg. Surg. 36 (6), 525–535.

Giannini, S., Leardini, A., O'Connor, J.J., 2000. Totoal ankle replacement - review of the design and the current status. Foot Ankle Surg. 6 (2), 77–88.

Kelikian, A. (Ed.), 2011. Sarrafian's Anatomy of the Foot and Ankle, Descriptive, Topographic, Functional. third ed. Lippincott Williams & Wilkins, Philadelphia.

Kimizuka, M., Kurosawa, H., Fukubayashi, T., 1980. Load-bearing pattern of the ankle joint. Contact area and pressure distribution. Arch. Orthop. Trauma Surg. 96 (1), 45–49.

Lapointe, S.J., Siegler, S., Hillstrom, H., Nobilini, R.R., Mlodzienski, A., Techner, L., 1997. Changes in the flexibility characteristics of the ankle complex due to damage to the lateral collateral ligaments: an in vitro and in vivo study. J. Orthop. Res. 15 (3), 331–341.

Leardini, A., O'Connor, J.J., Catani, F., Giannini, S., 1999b. Kinematics of the human ankle complex in passive flexion; a single degree of freedom system. J. Biomech. 32 (2), 111–118.

Leardini, A., O'Connor, J.J., Catani, F., Giannini, S., 1999a. A geometric model of the human ankle joint. J. Biomech. 32 (6), 585–591.

Lundberg, A., Goldie, I., Kalin, B., Selvik, G., 1989. Kinematics of the ankle/foot complex: plantarflexion and dorsiflexion. Foot Ankle 9 (4), 194–200.

Millington, S.A., Li, B., Tang, J., Trattnig, S., Crandall, J.R., Hurwitz, S.R., Acton, S.T., 2007b. Quantitative and topographical evaluation of ankle articular cartilage using high resolution MRI. J. Orthop. Res. 25 (2), 143–151.

Millington, S.A., Grabner, M., Wozelka, R., Anderson, D.D., Hurwitz, S.R., Crandall, J. R., 2007a. Quantification of ankle articular cartilage topography and thickness using a high resolution stereophotography system. Osteoarth. Cartilage 15 (2), 205–211.

Ringleb, S.I., Udupa, J.K., Siegler, S., Imhauser, C.W., Hirsch, B.E., Liu, J., Odhner, D., Okereke, E., Roach, N., 2005. The effect of ankle ligament damage and surgical reconstructions on the mechanics of the ankle and subtalar joints revealed by three-dimensional stress MRI. J. Orthop. Res. 23 (4), 743–749.

Siegler, S., Chen, J., Schneck, C.D., 1988. The three-dimensional kinematics and flexibility characteristics of the human ankle and subtalar joints–Part I: Kinematics. J. Biomech. Eng. 110 (4), 364–373.

Siegler, S., Lapointe, S., Nobilini, R., Berman, A.T., 1996. A six-degrees-of-freedom instrumented linkage for measuring the flexibility characteristics of the ankle joint complex. J. Biomech. 29 (7), 943–947.

Siegler, S., Udupa, J.K., Ringleb, S.I., Imhauser, C.W., Hirsch, B.E., Odhner, D., Saha, P. K., Okereke, E., Roach, N., 2005. Mechanics of the ankle and subtalar joints revealed through a 3D quasi-static stress MRI technique. J. Biomech. 38 (3), 567–578.

Sparmann, M., Wolke, B., Czupalla, H., Banzer, D., Zink, A., 2003. Positioning of total knee arthroplasty with and without navigation support. A prospective, randomised study. J. Bone Joint Surg. Br. 85 (6), 830–835.

Stormont, D.M., Morrey, B.F., An, K.N., Cass, J.R., 1985. Stability of the loaded ankle. Relation between articular restraint and primary and secondary static restraints. Am. J. Sports Med. 13 (5), 295–300.

Sugimoto, K., Takakura, Y., Tohno, Y., Kumai, T., Kawate, K., Kadono, K., 2005. Cartilage thickness of the talar dome. Arthroscopy 21 (4), 401–404.

Tochigi, Y., Rudert, M.J., Saltzman, C.L., Amendola, A., Brown, T.D., 2006. Contribution of articular surface geometry to ankle stabilization. J. Bone Joint Surg. Am. 88 (12), 2704–2713.

Please cite this article in press as: Siegler, S., et al. Analysis of surface-to-surface distance mapping during three-dimensional motion at the ankle and subtalar joints. J. Biomech. (2018), https://doi.org/10.1016/j.jbiomech.2018.05.026